J. Phycol. **44,** 541–550 (2008)

DOI: 10.1111/j.1529-8817.2008.00506.x

IMAGING OF OXYGEN DYNAMICS WITHIN THE ENDOLITHIC ALGAL COMMUNITY OF THE MASSIVE CORAL *PORITES LOBATA*[1]

Michael Kühl[2]

Marine Biological Laboratory, Department of Biology, University of Copenhagen, Strandpromenaden 5, DK-3000 Helsingør, Denmark

Gerhard Holst

PCO AG, Research & Development, Donaupark 11, D-93309 Kelheim, Germany

Anthony W. D. Larkum

School of Biological Sciences, University of Sydney, Sydney, New South Wales, Australia

and Peter J. Ralph

Institute for Water and Environmental Resource Management, University of Technology, Sydney, PO Box 123, Broadway 2007, New South Wales, Australia

We used transparent planar oxygen optodes and a luminescence lifetime imaging system to map (at a pixel resolution of <200 μm) the two-dimensional distribution of O_2 within the skeleton of a *Porites lobata* colony. The O_2 distribution was closely correlated to the distribution of the predominant endolithic microalga, *Ostreobium quekettii* Bornet et Flahault that formed a distinct green band inside the skeleton. Oxygen production followed the outline of the *Ostreobium* band, and photosynthetic O_2 production was detected at only 0.2 μmol photons $m^{-2} \cdot s^{-1}$, while saturation occurred at ~37 μmol photons $m^{-2} \cdot s^{-1}$. Oxygen levels varied from ~60% to 0% air saturation in the illuminated section of the coral skeleton in comparison to the darkened section. The O_2 production within the *Ostreobium* band was lower in the region below the upward facing surface of the coral and elevated on the sides. Oxygen consumption in darkness was also greatest within the *Ostreobium* zone, as well as in the white skeleton zone immediately below the corallites. The rate of O_2 depletion was not constant within zones and between zones, showing pronounced heterogeneity in endolithic respiration. When the coral was placed in darkness after a period of illumination, O_2 levels declined by 50% within 20 min and approached steady-state after 40–50 min in darkness. Our study demonstrates the use of an important new tool in endolith photobiology and presents the first data of spatially resolved O_2 concentration and its correlation to the physical structures and specific zones responsible for O_2 production and consumption within the coral skeleton.

Key index words: **endolithic; imaging; microenvironment; optode; *Ostreobium quekettii;* oxygen**

Abbreviations: **CCD, charge coupled device; *frac,* the fraction of quenchable indicator dye; I_0 and I, the luminescence intensity in the absence or presence of O_2; K_{SV}, the bimolecular quenching coefficient; LED, light emitting diode; $[O_2]$, oxygen concentration in percentage of air saturation; τ_0,τ, the luminescence lifetime (i.e., the decay time) in the absence or presence of O_2, respectively**

Endolithic phototrophic communities within scleractinic corals harbor mostly cyanobacteria, green algae, and photosynthetic bacteria (Le Campion-Alsumard et al. 1995, Gektidis et al. 2006, Ralph et al. 2007). The predominant endolithic algae belong to the siphonalean chlorophytes *Ostreobium* spp. (Phyllosiphoniaceae) that form conspicuous green bands inside living corals and as euendoliths are capable of actively dissolving the calcium carbonate when drilling into the coral skeleton (Highsmith 1981). Almost 98% of hermatypic corals contain green bands of *Ostreobium* (Le Campion-Alsumard et al. 1995). However, *Ostreobium* is not limited to the colored zones, as it can be present in most regions of the skeleton at densities insufficient to be visible (Le Campion-Alsumard et al. 1995).

Most endolithic algae occur within the outer 10–20 mm zone of the skeleton. *Ostreobium* penetrates to the bottom of the corallites, but its greatest density is toward the interior of the skeleton, so a distinctive green layer is usually seen several millimeters below and in parallel to the coral polyps (Halldal 1968, Jeffrey 1968). Highsmith (1981)

[1]Received 15 August 2007. Accepted 27 September 2007.
[2]Author for correspondence: e-mail mkuhl@bio.ku.dk.

determined that *Ostreobium* was further from the coral surface in the upper region of the colony than on the sides, suggesting that photoinhibition limits its location in the upper region.

The white zone often observed in between the green band and the tissue-containing corallites may be caused by photoinhibition of the upper *Ostreobium* band (Lukas 1974, Highsmith 1981), but the actual mechanism governing the formation of the white zone remains unresolved. Halldal (1968) observed only the ''most peripheral'' green band to be photosynthetically active, whereas Shibata and Haxo (1969) determined that insufficient light penetrated the outer green band to support photosynthesis, and the authors suggested that the inner bands may thus be inactive. In a recent study, we found multiple bands of photosynthetically active endoliths, both *Ostreobium* and cyanobacteria, in three species of corals (*Cyphastrea serailia*, *Porites lutea*, and *Goniastrea australensis*) (Ralph et al. 2007). These endolithic zones showed an extreme shade adaptation showing saturation of endolith photosynthesis at <10 μmol photons $\cdot$ m^{-2} $\cdot$ s^{-1}, as determined from variable fluorescence analysis.

Irradiance inside the coral skeleton is extremely low; usually <1% of available PAR at the coral surface actually reaches the *Ostreobium* zone (Shibata and Haxo 1969, Magnusson et al. 2007). The actual light intensity at the level of the endolithic algae has been estimated to reach <1–10 μmol photons $\cdot$ m^{-2} $\cdot$ s^{-1} (Schlichter et al. 1997). The light compensation point for *Ostreobium* was determined to be 10–50 μmol photons $\cdot$ m^{-2} $\cdot$ s^{-1}, and saturation was measured at irradiances of 35–200 μmol photons $\cdot$ m^{-2} $\cdot$ s^{-1} (Vooren 1981, Shashar and Stambler 1992, Schlichter et al. 1997, Magnusson 2006, Ralph et al. 2007). Schlichter et al. (1997) reported photoinhibition to occur at about 100 μmol photons $\cdot$ m^{-2} $\cdot$ s^{-1}. However, such irradiance levels would only reach the endolith zone in very shallow waters or in corals with damaged or bleached tissue (Fine et al. 2004, Magnusson et al. 2007).

The physical structure of the coral skeletal matrix provides a large area of substrate for endolithic communities to colonize, while its porous nature allows for, albeit limited, fluid and solute exchange (Risk and Müller 1983). Endolithic algae are adapted to diurnal fluctuations in pH and O_2 and a limited exchange of solutes with the water surrounding the coral colony (Shashar et al. 1997). Photosynthesis of the endolithic algae can alter the internal water chemistry of a coral colony. High O_2 production has been observed inside coral skeletons (Bellamy and Risk 1982), with O_2 and pH levels varying from ~200% of air saturation and pH 8.5 in light to <10% of air saturation and pH 7.7 in darkness (Shashar and Stambler 1992, M. Kühl unpublished data).

While endoliths within dead coral substrata are major primary producers on coral reefs (Larkum et al. 2003, Tribollet et al. 2006a,b), the magnitude and importance of endolithic primary production and respiration in living corals are not well understood. Shashar and Stambler (1992) observed very low endolithic respiration and photosynthesis rates accounting for maximally 3.5% of the total rates of intact corals, and they concluded that the chemical microenvironment in coral skeleton was mainly governed by coral tissue metabolism. Schlichter et al. (1997) showed that respiration of endolithic algae represented only 1.4% of the total colony respiration, while endolithic photosynthesis could account for 6% of a living coral colony. Recent studies indicate, however, that coral endoliths may translocate significant amounts of carbon to the coral and therefore can be of importance for coral host survival, for example, under conditions of coral bleaching (Fine and Loya 2002, Fine et al. 2004, 2005).

Oxygen concentration is tightly coupled to primary production; however, in mixed surface-associated photosynthetic communities, it is also strongly influenced by heterotrophic respiration (Kühl et al. 1996, Glud et al. 1999). Oxygen dynamics can be measured at high spatiotemporal resolution with O_2 microelectrodes and microoptodes (Kühl and Revsbech 2001, Kühl 2005). However, such measurements are only representative of a very small spatial scale, and for a complex sample, it would require a large number of replicates to map the heterogeneity. In a hard matrix such as coral skeleton, microsensor measurements require the drilling of a small (0.2–1 mm diameter) hole, and this may lead to artifacts as the diffusional geometry is changed.

A better method for spatial mapping of O_2 is based on the use of an optical oxygen indicator immobilized onto planar foils (so-called planar optodes). Such optical indicators exhibit a dynamic quenching when exposed to O_2 (i.e., the more O_2, the less luminescence). A two-dimensional distribution of an O_2-dependent luminescence signal over the foil can thus be monitored with a sensitive CCD camera system (Glud et al. 1996, Hartman and Ziegler 1996, Holst et al. 1998). This method allows the dynamic mapping of O_2 distribution under a range of light conditions across heterogeneous surfaces in laboratory experiments (Glud et al. 1999, Holst and Grunwald 2001) and in situ (Glud et al. 2001, Wenzhöfer and Glud 2004).

Initial applications to sediments used planar O_2 optodes with a black, yet O_2 permeable optical isolation in order to screen out optical artifacts due to ambient light or background fluorescence (Glud et al. 1996, 1999, König et al. 2001), and this prevented a direct comparison of sample structure and O_2 distribution. However, optical O_2 sensors exhibit O_2-dependent changes both in their luminescence intensity and in luminescence decay time (Klimant et al. 1999, Liebsch et al. 2000, Holst and Grunwald 2001). Luminescent indicators with decay times in the microsecond range allow the measurement of O_2 in samples with high levels of intrinsic fluorescence

(e.g., chl *a*), which usually decays completely within 100 ns (Govindjee et al. 1986) and therefore can be ignored. While luminescence intensity imaging requires optical isolation of planar optodes, imaging of the luminescence lifetime allows the use of transparent planar optodes (Holst et al. 1998, Holst and Grunwald 2001) for combined imaging of sample structure as well as O_2 dynamics.

In earlier papers, the spatial distribution and activity of endolithic microorganisms and their physicochemical microenvironment were addressed by reflectance spectroscopy, variable chl *a* fluorescence techniques (Grunwald and Kühl 2004, Ralph et al. 2007), and microscale light measurements with fiber-optic microprobes (Magnusson et al. 2007). In this study, we present the first application of transparent planar optodes to map the O_2 concentration and its dynamics within endolithic communities in the skeleton of the massive coral *P. lobata*. The focus of this study is methodological, and we did not attempt a comprehensive study with numerous replicates and subsequent statistical analysis. We demonstrate the potential of this new methodological approach to address the following specific questions: How do various endolithic zones respond to subsaturating irradiance? How does O_2 production align with the distribution of *Ostreobium*? And how rapidly is O_2 consumed in darkness from different regions within the coral skeleton?

MATERIALS AND METHODS

Coral samples. Samples of *P. lobata* were collected at low tide at <1 m water depth in Heron Island Lagoon (152°6′ E, 20°29′ S) and were maintained at Heron Island Research Station, University of Queensland, in an outdoor flow-through aquarium for 2 d under shaded conditions (max. irradiance of ~100 μmol photons · m^{-2} · s^{-1}) and constant flushing of fresh seawater from the lagoon. Samples were cut into halves through a medial longitudinal section using a diamond-tipped saw (10 cm blade, cooled by ample flushing with seawater) under shaded conditions. Samples were cut at the point of attachment and perpendicular to the coral surface, since this ensured that the samples were vertically oriented. Once the sample was cut, it was washed in seawater and placed on a sheet of black plastic to prevent light penetration through the cut surface and immediately placed in the experimental chamber. Data presented in a previous study (Ralph et al. 2007) showed that the activity of endoliths was not significantly inhibited or damaged by the described handling procedure. The major endolithic alga was identified as *O. quekettii* (Ralph et al. 2007). We used a relatively small colony of *P. lobata* (a length of about 6 cm along the longest axis) with a cut surface area of ~1,400 mm^2. The colony size was chosen to fit the given constraints of the imaging system, while at the same time being large (old) enough to have developed enough endolithic biomass.

Experimental setup. All experiments were performed in a darkened room at 20°C. A sectioned sample was placed in a 200 mL petri dish (with 0.45 μm filtered seawater) on top of a transparent planar oxygen optode (see below), and the dish was placed on top of a custom-built light-emitting diode (LED) array (Fig. 1). Water surrounding the sample was continuously aerated by a small stream of bubbles introduced to the top of the petri dish via a needle connected to an air pump. Water

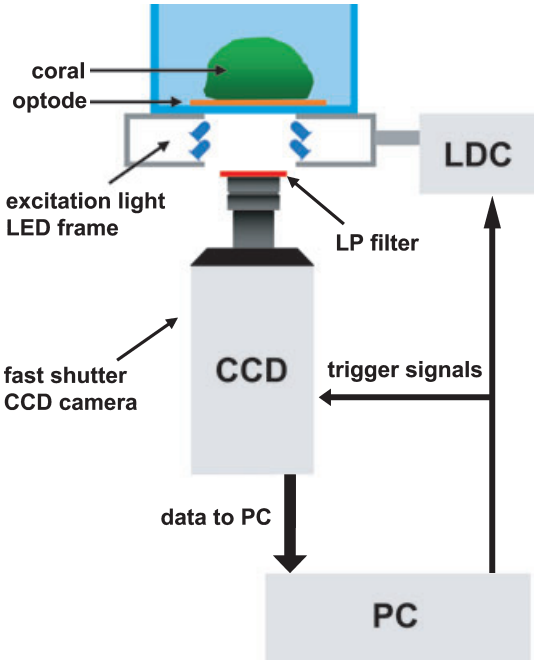

FIG. 1. Schematic diagram of the experimental setup: the sectioned coral lying on top of the transparent planar O_2 optode, fixed in place and filled with aerated seawater. The endolithic surface of the coral sample was illuminated through the planar optode by either (i) excitation light from the light-emitting diode (LED) array or (ii) a fiber-optic halogen lamp. The endolithic surface of the sectioned coral was imaged using a CCD camera equipped with a long-pass filter (LP) to screen out excitation light. A PC controlled the trigger signal timing for the LED array via an LED driving circuit (LDC) and captured the CCD images.

movement was impaired at the bottom surface of the petri dish, where the optode was in contact with the sectioned coral. The sample was fixed at the edges to the optode with Plasticine® (nontoxic) to achieve a waterproof contact between the coral surface and optode, preventing exchange of ambient oxygenated water across the sensor surface. Before experiments commenced, the petri dish was flushed with air until constant luminescent lifetime values were obtained (~30 min). During the following experiments, the endolith surface was imaged from below (see Fig. 1). At the end of the experiment, the sample was removed, and the sensor foil was calibrated by obtaining calibration images in nitrogen-flushed (0% saturation) and air-saturated seawater (100% air saturation), respectively.

The endolith surface was illuminated from the underside (through the optode) for 45 min over a range of actinic irradiances as provided by a fiber-optic halogen lamp (Ultralux 5000; Volpi, Schlieren, Switzerland) and quantified with a calibrated scalar irradiance meter (QSL-101; Biospherical Instruments, San Diego, CA, USA). Actinic illumination for ~45 min at each irradiance was sufficient to allow a steady-state O_2 level to develop across the surface of the skeleton. Once the sample reached steady-state conditions, O_2 images were recorded at a fast sampling rate (one image set per 4 s) for the first 2 min after darkening. For the next 6 min and onward, images were recorded at a slower sampling rate (one image set per minute). This sequence was repeated for each actinic irradiance (i.e., 0.2, 8.1, 19.8, 37.2, and 57.6 μmol photons · m^{-2} · s^{-1}). After 6 h of darkness, the chamber was illuminated from the side by a halogen lamp to record a monochrome structural image of the skeleton surface (Figs. 2A and 4A).

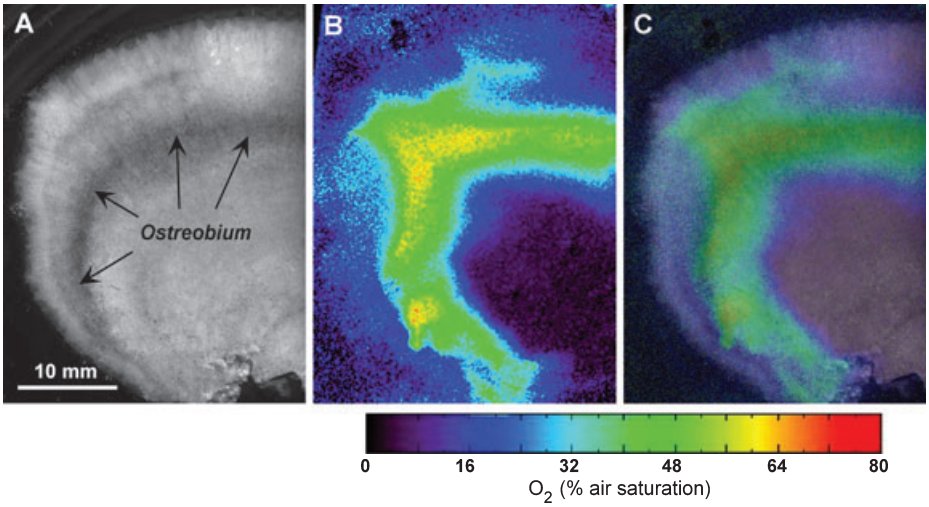

FIG. 2. (A) Monochrome image of the internal structure of a *Porites lobata* colony as seen through the optode. (B) Oxygen distribution over the same region illuminated with an irradiance of 57.6 μmol photons · m^{-2} · s^{-1}. (C) Superimposed images of structure and O_2 distribution. Oxygen values are given in % air saturation and are color coded between 0 and 80% air saturation. The colony is oriented with its natural upper surface oriented toward the top of the image.

These images of reflected light showed dark bands in the skeleton corresponding to strong absorption of light in the green zone of endolithic algae (Fig. 2).

Planar oxygen optode. We used a transparent O_2 optode (Holst and Grunwald 2001) in this investigation, whereas most earlier applications of O_2 optodes either contained scattering particles to enhance the signal (e.g., König et al. 2001) or were coated with an optical isolation of black silicone to isolate the signal from the ambient light (Holst et al. 1998, Glud et al. 1999, 2001, Liebsch et al. 2001). Visualization of the coral skeleton surface through the optode allowed us to easily align specific endolithic regions with the two-dimensional O_2 distribution image.

The planar O_2 sensor consisted of a luminescent oxygen indicator immobilized in a polystyrene matrix on a transparent polyester foil (Mylar Goodfellow, Huntingdon, UK). The measuring principle of planar optodes is based on the ability of O_2 to act as a dynamic quencher, which decreases the fluorescence quantum yield of an immobilized fluorophore (Demas 1976). The O_2 sensitive fluorophore was ruthenium(II)-tris-4,7-diphenyl-1,10-phenanthroline perchlorate with trimethylsilylpropanesulfonate as the counter ion (Hartmann and Leiner 1995, Mills and Thomas 1997). The fluorophore was excited by blue light from an LED array (peak excitation = 475 nm), and O_2-dependent red luminescent light (peak emission = 605–610 nm) was emitted by the indicator foil (Holst and Grunwald 2001). The presence of oxygen quenched the red emission of the fluorophore and shortened the luminescence decay time. A high-resolution CCD camera system for measuring luminescence lifetimes (Holst et al. 1998) imaged the distribution of the emitted red luminescence from the sensor foil (Fig. 1).

The oxygen quenching of the fluorophore signal is a nonlinear function of the O_2 concentration, which can be described by a two-component model of the Stern–Volmer equation (Carraway et al. 1991) modified such that the second component is assumed to be nonquenchable (Klimant et al. 1997, Holst and Grunwald 2001):

$$\frac{\tau}{\tau_0} = \frac{I}{I_0} = \left(\frac{\text{frac}}{(1 + K_{SV} \cdot [O_2])}\right) + (1 - \text{frac})$$

where τ_0 and τ denote the luminescence lifetime (i.e., the decay time) in the absence or presence of O_2, respectively; I_0 and I denote the luminescence intensity in the absence or presence of O_2, respectively; K_{SV} is the bimolecular quenching coefficient; $[O_2]$ denotes the O_2 concentration in percentage of air saturation; and frac is the fraction of quenchable indicator dye. For image processing, the variables τ_0, τ, K_{SV}, and $[O_2]$ in the formula were replaced by their corresponding images.

Image capture system. A modular luminescence lifetime imaging system (Holst et al. 1998; Fig. 1) was used to monitor the planar O_2 optode. The imaging system consists of a thermoelectrically cooled gate-able CCD camera (Sensicam-Sensimod VGA; PCO AG, Kelheim, Germany) with a special modulation input, allowing for an integration of charge carriers within the image sensor, and a controlling PC with an integrated timing board (Spectrum GmbH, Grosshansdorf, Germany). The modulated excitation light source consisted of an LED array (20 × blue LED, HLMP-CB15; Hewlett Packard, Palo Alto, CA, USA). A custom-built trigger unit generated the necessary timing signals to modulate the LED array, shutter, and image capture. The planar optode was imaged through a long pass filter (Deep Golden Amber; LEE Filter, Andover, UK) to remove any reflected light from the excitation source. A macro lens (Tevidon F1.4/f = 25 mm; Docter Optics, Neustadt a.d. Orla, Germany) focused the fluorescence image onto the CCD chip of the camera (Fig. 1). In this study, images covered an area of 54.0 × 40.5 mm (imaged with a resolution of 640 × 480 pixels). With the optical configuration used in this study, the spatial resolution was ~84 μm per pixel. In principle, both smaller and larger imaging areas can be realized by changing the front optics and the illumination geometry of the system (Holst and Grunwald 2001, Glud et al. 2001, Kühl et al. 2007).

Image acquisition. Actinic irradiance interfered with the luminescence measurement through the transparent foil. Therefore, image acquisition commenced immediately after the actinic illumination was switched off. To obtain O_2-dependent pictures of the luminescence lifetime, it is necessary to record sets of images with different time delays after turning off the excitation light (Holst et al. 1998). Software for controlling the image capture was written in *Delphi 4* (Inprise,

Scotts Valley, CA, USA). Briefly, the timing of events involved in the recording of a pair of lifetime images was as follows: First, the excitation light (LED array) was switched on for 4 μs. After 1 μs, the electronic shutter of the camera was opened for 3 μs and closed again after a further 7 μs (for total decay of the luminescence). This procedure was repeated up to 10,000 times, while the incident light was integrated onto the CCD chip, before the image was passed on to the PC. The next image followed the same process, only with a different time delay after the eclipse of the excitation light. In this way, the camera integrated the luminescence over specific regions of the decay curve. On the basis of the assumption that the luminescence decay curve follows a monoexponential decay (Hartmann et al. 1997, Holst and Grunwald 2001, Liebsch et al. 2001), it is possible to calculate the corresponding lifetime value using the two recorded images, corresponding to different parts of the luminescence decay curve (Holst et al. 1998). Shorter lifetimes indicate more O_2, while longer lifetimes indicate less O_2.

Image processing. Image processing of the recorded images was performed with a custom-made program (*MolliView* programmed with *IDL 5.4*; ITT Visual Information Solutions, Boulder, CO, USA). Every measurement consisted of a set of three files (two image files and a parameter file containing information about the timing scheme used). The calibration of measured image sets required two additional sets of images obtained at O_2 levels corresponding to 0% and 100% air saturation, respectively. First, each image set was converted into a two-dimensional array of real values of lifetimes (Holst et al. 1998, Holst and Grunwald 2001). When each image set was converted into lifetime array images, the two calibration images were used to calculate an image of the bimolecular quenching coefficient (K_{SV}). The zero O_2 lifetime image and the K_{SV} image were then used to convert the lifetime distribution images into O_2 images. All images were digitally smoothed by a running average of 2, which reduced the spatial resolution of the images from 84 μm to 168 μm per pixel. The resulting O_2 array images were color coded as isopleths of % air saturation and subsequently scaled for better visualization. A more detailed description of calibration and further image processing of lifetime images is given elsewhere (Holst and Grunwald 2001).

RESULTS

Using the O_2 production as a proxy, the distribution of endoliths over the sectioned surface of a *P. lobata* colony showed considerable heterogeneity over the sample area of ~1,400 mm^2 (Fig. 2). A visible and distinct 3–5 mm wide green band of predominantly *Ostreobium* was found 5–10 mm from the perimeter of the colony and corresponded with the distinct zone evident in the monochrome image (Fig. 2A). The O_2 distribution in the coral skeleton under illumination exhibited the highest values within the *Ostreobium* zone (Fig. 2B) as could be clearly seen when the O_2 distribution was superimposed on the structural picture of the coral (Fig. 2C). The O_2 distribution within the *Ostreobium* zone was heterogeneous, indicating zones of higher and lower photosynthetic activity and/or algal biomass. The upper surface of the coral was oriented toward the top of the images. It is apparent that *Ostreobium* showed elevated O_2 levels on the sides of the coral, as opposed to regions below the upper surface of the coral, where oxygen production was generally lower and further from the corallites.

The O_2 concentration and its distribution over the coral section responded strongly to increasing irradiance (Fig. 3). In the dark, the section was almost fully anoxic, but after 45 min exposure to 0.2 μmol photons $\cdot m^{-2} \cdot s^{-1}$, a small increase of O_2 was detected within certain parts of the *Ostreobium* zone. As the irradiance was further increased to 8.1 μmol photons $\cdot m^{-2} \cdot s^{-1}$, O_2 production was detected over most of the *Ostreobium* band and the white zone between the corallites and the *Ostreobium* band. After exposure to 19.8 μmol photons $\cdot m^{-2} \cdot s^{-1}$, the maximal O_2 level within the skeleton reached ~50% air saturation, and the distribution of O_2 correlated with the topology of the *Ostreobium* band. The O_2 distribution and concentration at the two highest irradiance levels (37.2 and 57.6 μmol photons $\cdot m^{-2} \cdot s^{-1}$, respectively) were similar, showing the first signs of decreasing O_2 levels in some areas.

We observed different patterns of O_2 consumption and production in different zones within the skeleton matrix. Four regions of identical area (30×60 pixels = 2.53×5.06 mm^2) were compared (Fig. 4A): Area 1 incorporated the innermost edge of the main *Ostreobium* band, area 2 was within the densest part of the *Ostreobium* band, area 3 contained the white zone between the *Ostreobium* band and the base of corallites, while area 4 included the base of corallites in the outermost skeleton layer.

All four regions showed a distinct increase of O_2 levels with irradiance, where areas 1 and 2 (i.e., the regions having the highest density of *Ostreobium*), reached the highest O_2 levels of ~40 ± 15% air saturation (Fig. 4B). The white zone (area 3) showed the smallest variation in oxygen with irradiance. Oxygen levels in the skeleton were constant at irradiances >37 μmol photons $\cdot m^{-2} \cdot s^{-1}$ indicating saturation of endolith photosynthesis.

The O_2 depletion after the onset of darkness also showed differences between the four areas (Fig. 5). In area 1, a very slow initial decline of O_2 after darkening was observed over a ~10 min lag phase followed by an increasing O_2 depletion rate that leveled off after ~30 min. Areas 2–4 showed an immediate and strong depletion of O_2 over the first 5 min after darkening, after which O_2 depletion rates decreased. Area 3 exhibited the fastest initial O_2 depletion rate. In areas 1–3, O_2 levels approached ~5% air saturation after about 60 min in darkness, while O_2 at the base of the corallites in area 4 was depleted to even lower levels of 0–2% air saturation.

Proximity to the coral tissue strongly influenced the consumption of O_2, but not the endolithic production of O_2. The lower edge of the *Ostreobium* zone (area 1) showed the slowest return to the previous O_2 level in darkness (dark steady state), indicating lower heterotrophic respiration in this zone. Whereas the

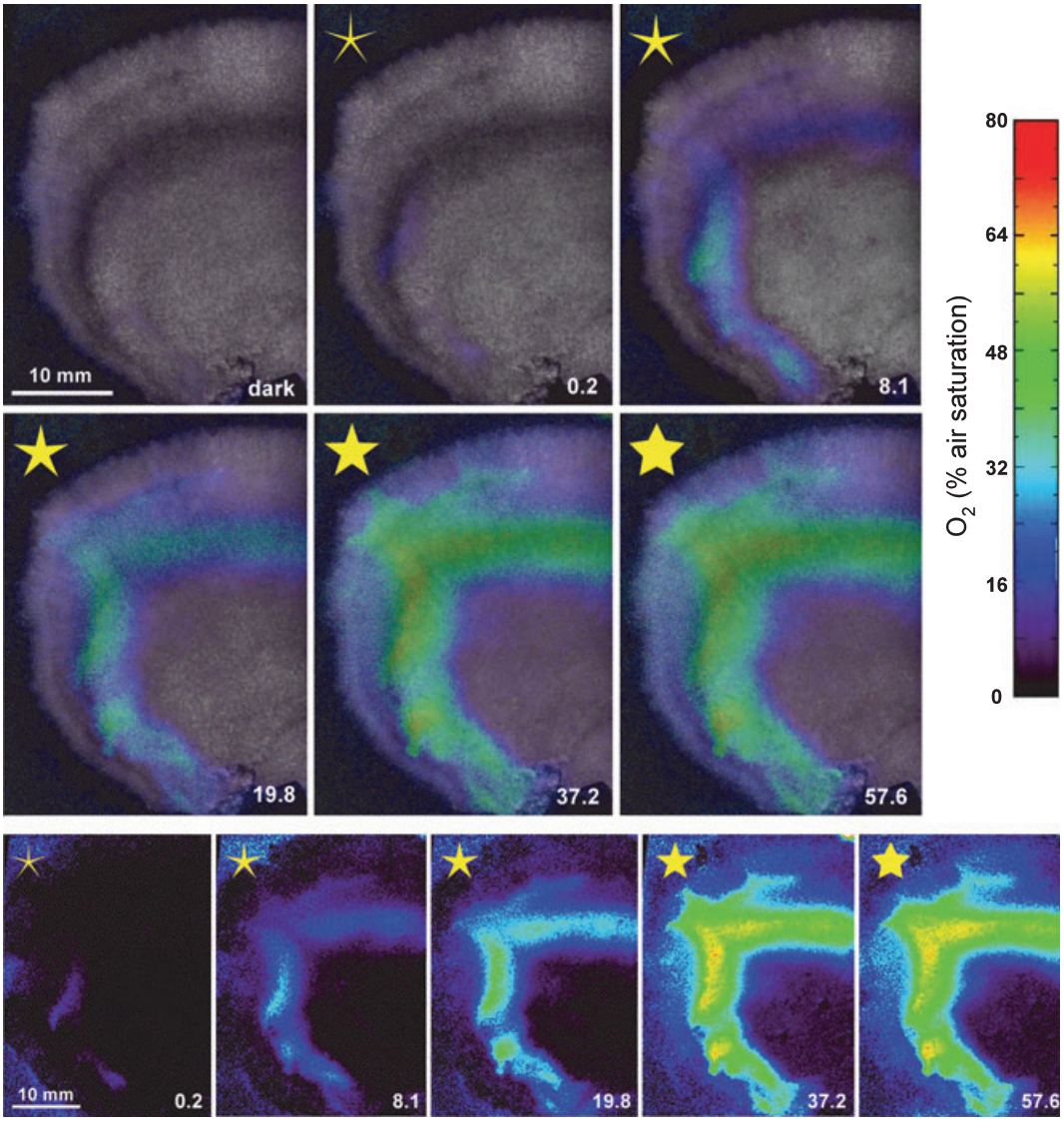

FIG. 3. Distribution of O_2 in the skeleton of *Porites lobata* in darkness and as a function of increasing incident irradiance (numbers on individual panels denote the irradiance in μmol photons · m^{-2} · s^{-1}). Both O_2 images (small panels) and O_2 images superimposed onto a monochrome image of the skeleton structure (large panels) are shown. Oxygen values are given in % air saturation and were color coded between 0 and 80% air saturation. The colony is oriented with its natural upper surface oriented toward the top of the image. Stars indicate irradiance level.

Ostreobium zone (area 2) showed a similar initial level of O_2 production as area 1 under saturating irradiance (57 μmol photons · m^{-2} · s^{-1}), the O_2 depletion was much faster and declined to the dark steady state within 20 min in the dense *Ostreobium* band, indicating higher respiration. Areas 3 and 4 had substantially less O_2 production after illumination, yet a rapid decline suggests a large potential for O_2 consumption, which could be associated with heterotrophic bacteria or coral polyp tissue.

DISCUSSION

This study is the first application of planar optodes for mapping O_2 dynamics in endolithic photosynthetic communities in corals. It presents the first data on the spatial distribution and dynamics of O_2 in a coral skeleton, in which we could superimpose distribution patterns of endolithic phototrophs and photosynthetic activity onto the skeleton structure.

Very few data on O_2 levels inside coral skeleton have been reported, and previous studies have relied on drilling holes into the skeleton matrix, wherein O_2 sensors were inserted (Shashar and Stambler 1992, Shashar et al. 1997, Magnusson 2006). These studies, representing a limited number of point measurements in the skeleton matrix, have shown that O_2 levels in coral skeleton vary between <10% and >200% air saturation in darkness and high irradiance, respectively. Furthermore, the dynamics were determined to be very slow during

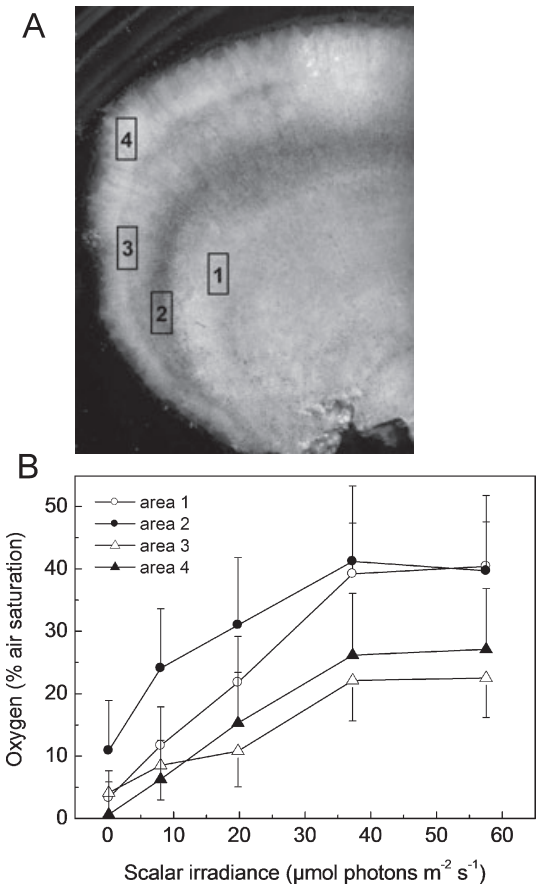

FIG. 4. Oxygen levels as a function of irradiance within four different regions in the skeleton of *Porites lobata* (A) corresponding to an area below the *Ostreobium* band (area 1), in the dense green *Ostreobium* layer (area 2), in the white zone in between the *Ostreobium* and the surface skeleton layers (area 3), and in the uppermost part of the skeleton containing corallites of *P. lobata* (area 4). (B) Oxygen levels are shown as % air saturation, with symbols and error bars representing mean and SDs of pixels (n = 1,800) within each area. The colony is oriented with its natural upper surface oriented toward the top of the image.

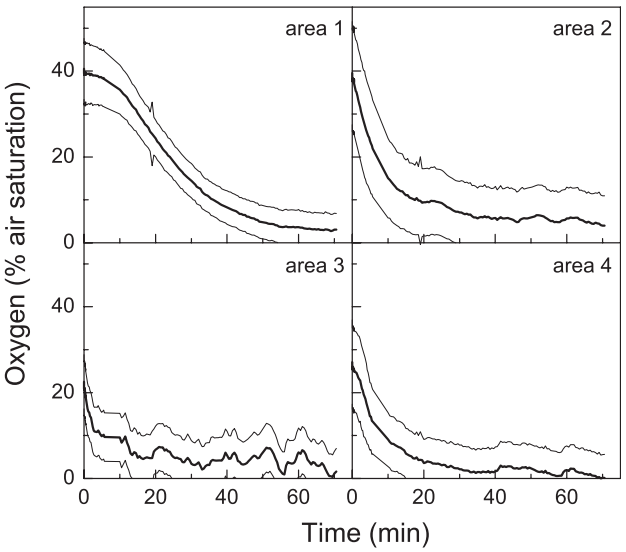

FIG. 5. Oxygen dynamics measured within four different regions in the skeleton of *Porites lobata* (see Fig. 4A) starting after 45 min exposure to 57.6 µmol photons · m^{-2} · s^{-1} and then followed for 70 min after darkening. Oxygen levels are shown as % air saturation. The thick curves show the mean O_2, while the thin curves outline the SD of pixels (n = 1,800) within each area.

experimental light:dark (L:D) cycles (i.e., in the range of hours) and were thus affected by diffusional exchange of O_2 with the coral tissue and the water in the drill hole (Magnusson 2006). As light was applied externally to the coral surface, earlier measurements characterized the combined effect of coral tissue and endoliths on the O_2 conditions in the skeleton, and coral metabolism was found to predominate the chemical microenvironment in the skeleton (Shashar and Stambler 1992).

Our study focused on the O_2 dynamics due to endolithic photosynthesis and respiration in the skeleton, and here, illumination of the skeleton through the planar optode was advantageous as it did not stimulate coral tissue photosynthesis significantly (Fig. 3). Planar optode measurements with illumination via the coral surface would, however, show the overall O_2 dynamics in living coral skeleton, as the internal O_2 level is determined not only by endolithic activity but also by the dynamic O_2 exchange in the coral tissue layer. Such studies remain to be conducted.

We illuminated the exposed skeleton through the transparent planar optode foil, consequently filtering out shorter wavelengths. The photosynthetic response of the endolithic community might thus be different if exposed to a broader spectral illumination. However, the spectral composition of light traveling in the skeleton shifts dramatically with distance from the coral surface. Light reaching the green endolithic zone is highly depleted in visible wavelengths that are strongly absorbed in the coral tissue, while far-red light penetrates efficiently through the tissue layer (Magnusson et al. 2007). One way of accounting for such spectral effects when measuring O_2 distributions could again be to illuminate the endoliths from outside via the coral surface and then monitor the resulting O_2 distribution in the skeleton compared to results when illuminating the coral slab via the O_2 optode. This does, however, require a more sophisticated experimental setup than used in this study, so as to minimize stray light in the chamber reaching the exposed endoliths when illuminating the endoliths through the coral surface. It would also require a precise quantification of the irradiance penetrating through the skeleton to the endolith layers monitored by the planar optode.

The spatial distribution of *Ostreobium quekettii* was closely correlated with regions of highest O_2 production (Fig. 3). However, within the *Ostreobium* band there was considerable variation in O_2

production. This finding may be linked to local variation in algal density (Le Campion-Alsumard et al. 1995), microbial respiration, or water movement. If the surface of the sectioned coral was not flat, water (with unknown O_2 content) could move preferentially through channels or into reservoirs. This possibility seems unlikely, however, as none of the images showed plumes of water with slowly varying O_2 content. Diffusive exchange of O_2 with the porous skeletal matrix is also possible, but this would be relatively constant over the cut surface, unless structures such as corallites influence the internal passage of water.

Orientation of the colony influenced the O_2 production within the *Ostreobium* band. The zones of *Ostreobium* and O_2 production were further from the upward-facing surface of the colony than from the sides (Figs. 2A and 3). This effect is probably related to light penetration. Highsmith (1981) observed that vertically directed corallites on the top of coral colonies had a better ability to guide light deeper into the coral skeleton than corallites on the side of the colony, where sunlight would always enter a corallite at an angle, thereby reducing light penetration into the skeleton and limiting endolithic photosynthesis closer to the surface.

The endolithic phototrophic community in *P. lobata* was well adapted to extreme shade conditions, as evidenced by a detectable O_2 production at extremely low irradiance (0.2 μmol photons $\cdot m^{-2} \cdot s^{-1}$) (Fig. 3). Oxygen levels in the skeleton increased rapidly with irradiance but did not change at >37 μmol photons $\cdot m^{-2} \cdot s^{-1}$, indicating that endolith photosynthesis was saturated at low irradiance (Figs. 3 and 4). In a recent study, we used chl variable fluorescence analysis to investigate the photosynthetic activity as a function of irradiance in *P. lobata* and two other massive corals and observed saturation of PSII electron transport at irradiances of <10 μmol photons $\cdot m^{-2} \cdot s^{-1}$ (Ralph et al. 2007). In other studies, Schlichter et al. (1997) found saturation of photosynthesis at 35–40 μmol photons $\cdot m^{-2} \cdot s^{-1}$, while Shashar and Stambler (1992) reported saturation at ~160 μmol photons $\cdot m^{-2} \cdot s^{-1}$. However, the latter studies used polarographic O_2 measurements and chamber incubations of intact coral colonies, and the light at the level of the endoliths was not quantified.

Oxygen levels in the coral skeleton are affected by endolithic metabolism and solute exchange with the coral tissue-containing part of the colony that also exhibits pronounced light-driven oxygen dynamics (Kühl et al. 1995, De Beer et al. 2000). A relatively fast O_2 depletion after the actinic light was switched off (Fig. 5) indicated significant respiratory activity in the skeleton that leveled out over time probably due to depletion of easily degradable substrate. The largest reduction in oxygen was found in area 4 closest to the coral polyp tissue, and it is likely that respiratory demands of the coral could be depleting the endolith oxygen production more rapidly than in other regions. Microbial respiration within the skeleton of corals has been inferred by reduced pH and O_2 concentrations within coral head porewater (Risk and Müller 1983), but the regulation of endolith respiration and the dynamics of respiratory substrates in the coral skeleton have not been studied.

We demonstrated that the majority of endolithic O_2 production of a living coral colony was closely linked to the distribution of the predominating endolithic alga, *O. quekettii*. The green *Ostreobium* zone generated sufficient O_2 production to be detected at 0.2 μmol photons $\cdot m^{-2} \cdot s^{-1}$, and O_2 production was saturated at >37 μmol photons $\cdot m^{-2} \cdot s^{-1}$ (Figs. 3 and 4). Oxygen imaging thus allowed us to map the spatial distribution and heterogeneity of O_2 production within the different endolithic regions of this coral. The rapid loss of O_2 after the L:D transition reflects a high respiratory activity within the coral skeleton (Fig. 5). The speed of O_2 depletion was not constant within zones and between zones (Fig. 5), implying a heterogeneous distribution of endolithic microorganisms and their rate of metabolism. Whether this is due to structural heterogeneity affecting mass transfer in the skeleton matrix or a patchy distribution of endolithic auto- and heterotrophs and respiratory substrates in the coral skeleton awaits further studies, where the spatial oxygen dynamics is, for example, coupled with microscopic mapping of microbial biomass and small-scale analysis of organic carbon pools.

In principle, images of the O_2 dynamics after darkening could be used to calculate images of gross photosynthetic rate from the rate of O_2 depletion (see Glud et al. 1999), analogous to the oxygen microsensor L:D shift method (Revsbech and Jørgensen 1983). The L:D shift method relies on determination of the initial O_2 depletion rate within <1–2 s after darkening. Images can be acquired at subsecond time intervals with the camera system used in this study. However, the response time of planar optodes is typically in the range of seconds, which will tend to obscure the real distribution of gross photosynthetic activity and decrease the spatial resolution (Glud et al. 1999). Furthermore, thick sensor layers can act as a reservoir for O_2, allowing for lateral diffusion in the planar optode matrix, which causes additional smearing effects and decreased spatial resolution. A more accurate determination of gross photosynthesis with planar optodes thus requires thin and fast-responding sensor foils and a quantification of horizontal diffusion in the sensor layer. It was not the aim of this study to perform such sensor optimizations, but the use of transparent planar optodes, without the 20–40 μm thick optical isolation of black silicone used in earlier photosynthetic studies presents a

clear advantage in terms of shorter response time and smaller susceptibility for smearing effects.

We have recently developed ultrathin (<1–2 μm thick) and homogeneous O_2-sensitive coatings with ideal quenching behavior and μm spatial resolution (Kühl et al. 2007). Such fast-responding planar O_2 optodes should be ideal for photosynthesis measurements, especially when combined with more advanced imaging protocols for time-resolved O_2 dynamics (Polerecky et al. 2005) and, for example, variable chl fluorescence imaging of endolith photosynthesis (Grunwald and Kühl 2004). Besides O_2 imaging, sensor materials and imaging systems for pH and CO_2 mapping in environmental samples have become available (Liebsch et al. 2000, 2001, Zhu et al. 2005, 2006, Stahl et al. 2006) and may also prove useful for endolith research.

Further application of planar optodes for studies of the microenvironment and chemical dynamics in coral skeletons is now underway. Such studies are important for obtaining a better understanding of the abiotic and biotic processes in coral skeleton that shape the endolithic microenvironment, and planar optodes seem a powerful method to, for example, resolve the effects of coral bleaching (Fine et al. 2004, 2005) or rising CO_2 levels (Tribollet et al. 2006a,b) on endolithic communities of coral reefs. The experimental approach demonstrated in this study of coral endoliths is also very promising for future studies of other hard substrata harboring photosynthetic microbes, which are difficult, or impossible, to investigate with microsensors. This possibility includes, for example, stromatolites, hard plant and animal tissues, and terrestrial endolithic communities (Büdel et al. 2004).

This study was supported by the Danish Natural Science Research Council and the Danish Research Council for Technology and Production Sciences (M. K.), the Max-Planck Society (G. H.), UTS Internal Funds (P. J. R.), and the Australian Research Council (P. J. R., A. W. D. L., M. K.). Ingo Klimant generously provided the planar oxygen sensors used in this study. Björn Grunwald is thanked for technical advice and assistance in developing the oxygen-imaging software. Roland Thar provided excellent assistance in the final graphics design of the illustrations. We wish to thank the staff at Heron Island Research station for their support and assistance in this research. All work was carried out under Queensland National Parks and Wildlife Service collection permit G01/623.

Bellamy, N. & Risk, M. J. 1982. Coral gas: oxygen production in *Millipora* on the Great Barrier Reef. *Science* 215:1618–9.

Büdel, B., Weber, B., Kühl, M., Pfanz, H., Sültemeyer, D. & Wessels, D. 2004. Reshaping of sandstone surfaces by cryptoendolithic cyanobacteria: bioalkalisation causes chemical weathering in arid landscapes. *Geobiology* 2:261–8.

Carraway, E. R., Demas, J. N., DeGraff, B. A. & Bacon, J. R. 1991. Photophysics and photochemistry of oxygen sensors based on luminescent transition-metal complexes. *Anal. Chem.* 63: 337–42.

De Beer, D., Kühl, M., Stambler, N. & Vaki, L. 2000. A microsensor study of light enhanced Ca^{2+} uptake and photosynthesis in the reef-building coral *Favia* sp. *Mar. Ecol. Prog. Ser.* 194:75–85.

Demas, J. N. 1976. Luminescence decay times and bimolecular quenching. *J. Chem. Educ.* 53:657–63.

Fine, M. & Loya, Y. 2002. Endolithic algae – an alternative source of energy during coral bleaching. *Proc. R. Soc. Lond. B Biol. Sci.* 269:1205–10.

Fine, M., Meroz-Fine, E. & Hoeg-Guldberg, O. 2005. Tolerance of endolithic algae to elevated temperature and light in the coral *Montipora monasteriata* from the southern Great Barrier Reef. *J. Exp. Biol.* 208:75–81.

Fine, M., Steindler, L. & Loya, Y. 2004. Endolithic algae photoacclimate to increased irradiance during coral bleaching. *Mar. Freshw. Res.* 55:115–21.

Gektidis, M., Dubinsky, Z. & Goffredo, S. 2006. Microendoliths of the shallow euphotic zone in open and shaded habitats at 30°N – Eilat, Israel – paleoecological implications. *Facies* 53:43–55.

Glud, R. N., Kühl, M., Kohls, O. & Ramsing, N. B. 1999. Heterogeneity of oxygen production and consumption in a photosynthetic microbial mat as studied by planar optodes. *J. Phycol.* 35:270–9.

Glud, R. N., Ramsing, N. B., Gundersen, J. K. & Klimant, I. 1996. Planar optrodes: a new tool for fine scale measurements of two-dimensional O_2 distribution in benthic communities. *Mar. Ecol. Prog. Ser.* 140:217–26.

Glud, R. N., Tengberg, A., Kühl, M., Hall, P., Klimant, I. & Holst, G. 2001. An *in situ* instrument for planar O_2 optode measurements at benthic interfaces. *Limnol. Oceanogr.* 46:2073–80.

Govindjee, Amesz, J. & Fork, D. C. 1986. *Light Emission by Plants and Bacteria.* Academic Press, Orlando, Florida, 635 pp.

Grunwald, B. & Kühl, M. 2004. A system for imaging variable chlorophyll fluorescence of aquatic phototrophs. *Ophelia* 58:79–89.

Halldal, P. 1968. Photosynthetic capacities and photosynthetic action spectra of endozoic algae of the massive coral *Favia. Bull. Mar. Biol. Lab. Woods Hole* 134:411–24.

Hartmann, P. & Leiner, M. J. P. 1995. Luminescence quenching behavior of an oxygen sensor based on a Ru(II) complex dissolved in polystyrene. *Anal. Chem.* 67:88–93.

Hartmann, P. & Ziegler, W. 1996. Lifetime imaging of luminescent oxygen sensors based on all-solid-state technology. *Anal. Chem.* 68:4512–4.

Hartmann, P., Ziegler, W., Holst, G. & Lübbers, D. W. 1997. Oxygen flux fluorescence lifetime imaging. *Sens. Act. B* 38:110–5.

Highsmith, R. C. 1981. Lime-boring algae in hermatypic coral skeletons. *J. Exp. Mar. Biol.* 55:267–81.

Holst, G. & Grunwald, B. 2001. Luminescence lifetime imaging with transparent oxygen optodes. *Sens. Act. B* 74:78–90.

Holst, G., Kohls, O., Klimant, I., König, B., Kühl, M. & Richter, T. 1998. A modular luminescence lifetime imaging system for mapping oxygen distribution in biological samples. *Sens. Act. B* 51:163–70.

Jeffrey, S. W. 1968. Pigment composition of siphonales algae in the brain coral *Favia. Biol. Bull.* 135:141–8.

Klimant, I., Kühl, M., Glud, R. N. & Holst, G. 1997. Optical measurement of oxygen and temperature in microscale: strategies and biological applications. *Sens. Act. B* 38–39:29–37.

Klimant, I., Ruckruh, F., Liebsch, G., Stangelmayer, A. & Wolfbeis, O. S. 1999. New soluble ormosils and their application in lifetime based oxygen microsensing. *Mikrochim. Acta* 131: 35–46.

König, B., Holst, G., Kohls, O., Richter, T., Glud, R. N. & Kühl, M. 2001. Imaging of oxygen distribution at benthic interfaces: a brief review. *In* Aller, J. Y., Woodin, S. A. & Aller, R. C. [Eds.] *Organism–Sediment Interactions.* University of South Carolina Press, Columbia, South Carolina, pp. 63–73.

Kühl, M. 2005. Optical microsensors for analysis of microbial communities. *In* Leadbetter, J. R. [Ed.] *Environmental Microbiology. Methods Enzymol.* 397:166–99.

Kühl, M., Cohen, Y., Dalsgaard, T., Jørgensen, B. B. & Revsbech, N. P. 1995. The microenvironment and photosynthesis of zooxanthellae in scleractinian corals studied with microsensors for O_2, pH and light. *Mar. Ecol. Prog. Ser.* 117:159–72.

Kühl, M., Glud, R. N., Ploug, H. & Ramsing, N. B. 1996. Microenvironmental control of photosynthesis and photosynthesis-coupled respiration in an epilithic cyanobacterial biofilm. *J. Phycol.* 32:799–812.

Kühl, M. & Revsbech, N. P. 2001. Biogeochemical microsensors for boundary layer studies. *In* Boudreau, B. P. & Jørgensen, B. B. [Eds.] *The Benthic Boundary Layer.* Oxford University Press, Oxford, UK, pp. 180–210.

Kühl, M., Rickelt, L. F. & Thar, R. 2007. Combined imaging of oxygen and bacteria in biofilms. *Appl. Environ. Microbiol.* 73:6289–95.

Larkum, A. W. D., Koch, E. M. & Kühl, M. 2003. Diffusive boundary layers and photosynthesis of the epilithic algal community of coral reefs. *Mar. Biol.* 142:1073–82.

Le Campion-Alsumard, T., Golubic, S. & Hutchings, P. 1995. Microbial endoliths in skeletons of live and dead corals: *Porites lobata* (Moorea, French Polynesia). *Mar. Ecol. Prog. Ser.* 117:149–57.

Liebsch, G., Klimant, I., Frank, B., Holst, G. & Wolfbeis, O. S. 2000. Luminescence lifetime imaging of oxygen, pH and carbon dioxide using optical sensors. *Appl. Spectrosc.* 54:548–59.

Liebsch, G., Klimant, I. & Wolfbeis, O. S. 2001. Fluorescent imaging of pH with optical sensors using time domain dual lifetime referencing (t-DLR). *Anal. Chem.* 73:4354–63.

Lukas, K. J. 1974. Two species of the chlorophyte genus *Ostreobium* from skeletons of Atlantic and Caribbean reef corals. *J. Phycol.* 10:331–5.

Magnusson, S. H. 2006. The microenvironment of endolithic phototrophs in the skeletons of scleractinians corals. M.Sc. thesis, Marine Biological Laboratory, Department of Biology, University of Copenhagen, Denmark, 72 pp.

Magnusson, S. H., Fine, M. & Kühl, M. 2007. Light microclimate of endolithic phototrophs in the scleractinian corals *Montipora monasteriata* and *Porites cylindrica*. *Mar. Ecol. Prog. Ser.* 332:119–28.

Mills, A. & Thomas, M. 1997. Fluorescence-based thin plastic film ion-pair sensors for oxygen. *Analyst* 122:63–8.

Polerecky, L., Franke, U., Werner, U., Grunwald, B. & De Beer, D. 2005. High spatial resolution measurements of oxygen consumption rates in permeable sediments. *Limnol. Oceanogr. Methods* 3:75–85.

Ralph, P. J., Larkum, A. W. D. & Kühl, M. 2007. Photobiology of endolithic microorganisms in living coral skeletons: 1. Pigmentation, spectral reflectance and variable chlorophyll fluorescence analysis of endoliths in the massive corals *Cyphastrea serailia*, *Porites lutea* and *Goniastrea australensis*. *Mar. Biol.* 152:395–404.

Revsbech, N. P. & Jørgensen, B. B. 1983. Photosynthesis of benthic microflora measured with high spatial resolution by the oxygen microprofile method: capabilities and limitations of the method. *Limnol. Oceanogr.* 28:749–56.

Risk, M. J. & Müller, H. R. 1983. Porewater in coral heads: evidence for nutrient regeneration. *Limnol. Oceanogr.* 28:1004–8.

Schlichter, D., Kampmann, H. & Conrady, S. 1997. Trophic potential and photoecology of endolithic algae living within coral skeletons. *P.S.Z.N. Mar. Ecol.* 18:299–317.

Shashar, N., Banaszak, A. T., Lesser, M. P. & Amrami, D. 1997. Coral endolithic algae: life in a protected environment. *Pac. Sci.* 51:167–73.

Shashar, N. & Stambler, N. 1992. Endolithic algae within corals – life in an extreme environment. *J. Exp. Mar. Biol. Ecol.* 163: 277–86.

Shibata, K. & Haxo, F. T. 1969. Light transmission and spectral distribution through epi- and endozoic algal layers in the brain coral, *Favia*. *Biol. Bull.* 136:461–8.

Stahl, H., Glud, A., Schröder, C. R., Klimant, I., Tengberg, A. & Glud, R. N. 2006. Time-resolved pH imaging in marine sediments with a luminescent optode. *Limnol. Oceanogr. Methods* 4:336–45.

Tribollet, A., Atkinson, M. J. & Langdon, C. 2006b. Effects of elevated pCO_2 on epilithic and endolithic metabolism of reef carbonates. *Glob. Change Biol.* 12:2200–8.

Tribollet, A., Langdon, C., Golubic, S. & Atkinson, M. 2006a. Endolithic micro-flora are major primary producers in dead carbonate substrates of Hawaiian coral reefs. *J. Phycol.* 42:292–303.

Vooren, C. M. 1981. Photosynthetic rates of benthic algae from the deep coral reef of Curacao. *Aquat. Bot.* 10:143–54.

Wenzhöfer, F. & Glud, R. N. 2004. Small-scale spatial and temporal variability in coastal benthic O_2 dynamics: effects of fauna activity. *Limnol. Oceanogr.* 49:1471–81.

Zhu, Q., Aller, R. C. & Fan, Y. 2005. High-performance planar pH fluorosensor for two-dimensional pH measurements in marine sediment and water. *Environ. Sci. Technol.* 39:8906–11.

Zhu, Q., Aller, R. C. & Fan, Y. 2006. A new ratiometric, planar fluorosensor for measuring high resolution, two-dimensional pCO_2 distributions in marine sediments. *Mar. Chem.* 101: 40–53.